HiSST: International Conference on
High-Speed Vehicle Science Technology
26–29 November 2018, Moscow, Russia

# Three-dimensional bump design for improving the starting characteristic of hypersonic inlets

*Xiaogang Zheng[1], Yiqing Li[2], Chengxiang Zhu[3], Yancheng You**

**School of Aerospace Engineering, Xiamen University, Xiamen, 361102, China**

## Abstract

A three-dimensional bump was generated based on the theory of conical waverider at Mach 6，which was applied to analyse the internal and external flow field as well as the low-speed starting characteristic of hypersonic inlets. The effect of separation control was discussed in detail. And the effect of 3D bump on the lift-drag characteristic of hypersonic inlet was considered as well. The results showed that the designed 3D bumps based on the theory of conical flow can play an effective role in boundary layer displacement. An optimized 3D bump can improve the low-speed starting characteristic of the inlet as the captured boundary layer is reduced by 9.3%, and meanwhile the lift-drag ratio is increased by 16.7%.

**Keywords**: *bump; boundary layer displacement; hypersonic inlet, starting characteristic; lift-to-drag ratio*

## 1. Introduction

The last few decades have been witnessed a growing trend towards hypersonic inlet, which need to provide a steady stream of compressed air to the compressor face of an engine over a wide range of speeds, altitudes and maneuvering conditions. Hence, hypersonic vehicles encounter a variety of freestream disturbances in pressure, temperature and velocity during whole flight [1]. All these disturbances especially in low speed can cause expulsion of the normal shock from the hypersonic inlet, also known as inlet unstart. If not avoided efficiently, an unstart results in a loss of propulsive efficiency and is able to cause in-flight engine malfunctioning [2-5]. In 1966, a hybrid engine (turbojet and ramjet) powered air fighter (SR-71 Blackbird) capable of Mach 3.2 flight at 80,000 ft crashed due to engine cutoff induced by this inlet unstart.

Then, in a ground test facility that mimics the thermal choking by the downstream movement of a mechanical flap, Wanger et al. [6] confirmed the presence of the separated boundary layer using PIV and Hyungrok et al found that the presence of turbulent wall boundary layers strongly affect the unstart dynamics [7]. These results confirm the importance of and need to remove the upstream low-kinetic flow to improve the starting characteristics of hypersonic inlets.

Past studies have examined methods such as the introduction of isolators [8-11], boundary layer bleeding system [12], and vortex generator jets [13], as a means of avoiding or delaying inlet unstart. The latter two approaches seek to influence the evolution of the low-kinetic flow during the upstream propagation of the flow disturbances that originate from the combustor. However, the bulk of these methods require complicated control system, which tends to increase the weight as well as complication of high speed vehicles.

The concept of a three-dimensional surface for use in supersonic inlet has been investigated before. Simen et al [14] studied an external bump-type inlet with boundary layer bleeding, which yields satisfactory operational stability over arrange of Mach number from 1.5 to 2.0. It is expected that the

[1] *School of Aerospace Engineering Xiamen University, China, xiaogangzheng@stu.xmu.deu.cn*
[2] *School of Aerospace Engineering Xiamen University, China, 12529000@qq.com*
[3] *School of Aerospace Engineering Xiamen University, China, chengxiang.zhu@xmu.edu.cn*
** School of Aerospace Engineering Xiamen University, China, yancheng.you@xmu.edu.cn*

innovative features of a bump-type inlet will remove the boundary layer with the effectiveness nearing that of a conventional ramp-type inlet, but without the complex and heavy mechanical bleeding systems. Seddon and Goldsmith [15] described the bump intake as a novel device. They cited Ferri [16] as suggesting that a bump-compression surface could be formed by tracing fluid streamlines through the flow field of a cone and noted that such a design had been adopted for use in the Grumman Super-Tiger aircraft.

Gridley and Cahill [17] discussed the Advanced Compact Inlet System program, which was dedicated in part to the analysis of several fundamentally different compression systems. The bump inlet performed comparably with a 2D waverider inlet while reducing weight suffering from less drag and maintaining ease of fabrication. Detail numerical studies have been conducted by Kim and Song [18], and the results showed that it is possible to optimize a three-dimensional bump which improves the performance of a mixed compression intake. Additionally, Eiman B. Saheby [19] proposed a novel concept for highly integrated intakes based on the theory of three-dimensional bump. This concept, called "Ridge", is an aerodynamic surface, involving a vortex and pressure gap to redirect the low-kinetic flow.

Extensive researches have shown that the azimuthal pressure gradient on the bump-compression surface plays a critical role in removing a majority of boundary layer from the inlet. Up to now, a considerable amount of literature has been published on the use of bump for supersonic inlet. However, there are no published studies that have made a detailed research on the three-dimensional bump-compression surface designed for high speed vehicles. Consequently, this study seeks to obtain data which will help to address these research gaps. And enlightened by the extensive application of Diverterless Supersonic Inlet (DSI) [20], a bump-compression surface is applied in hypersonic inlet so that the starting characteristics of hypersonic inlet can be optimized.

This paper describes a study of the unstart in a hypersonic model inlet. Primarily, a cone-derived bump is installed in a typical hypersonic inlet. Then, the flow structures of the original model and the model with bump are discussed under the design condition and off-design condition. The influence of bump-compression surface on the starting characteristics of hypersonic inlet therefore is explored in detail. In addition, the influence of bump on the integrated lift and drag coefficient under design and off-design condition is taken into account as well.

## 2. Bump design theory and numerical approach

### 2.1. Design theory of bump-compression surface

As mentioned above, the three-dimensional bump-compression surface applied in the DSI inlet could be derived by tracing fluid streamlines through the flow field of a cone at zero incidence. A general procedure of generating a bump-compression surface is shown in Fig.1. To begin with, a slender axisymmetric cone with its axis aligned in the direction of a hypersonic freestream is assigned firstly and then the flow filed can be constructed rapidly and accurately by solving the Taylor-Maccoll flow government equations [21, 22], which is an exact method. Next, a flow capture tube (FCT) may be arbitrarily defined whose intersection with the shock surface defines the leading edge of the bump. If a particle is released from each spanwise station along this leading edge and integrated to a sufficient distance downstream, the bump-compression surface is formed by the resulting traces.

Consequently, when the DSI inlet works under the design conditions, the flow field generated by the compression surface is still a conical flow filed with the conical shock attached to the leading edge. Due to the basic characteristics of the conical flow field, there are strong adverse and azimuthal pressure gradient on the bump surface. And it is expected that their combined action will remove most of the boundary layer out of the inlet effectively, but without the complex and heavy mechanical bleeding systems. What's more, the shape of the conical shock is supposed to be adjusted properly to match the complicate inlet lips so that the mass flow coefficient can be improved to some extent.

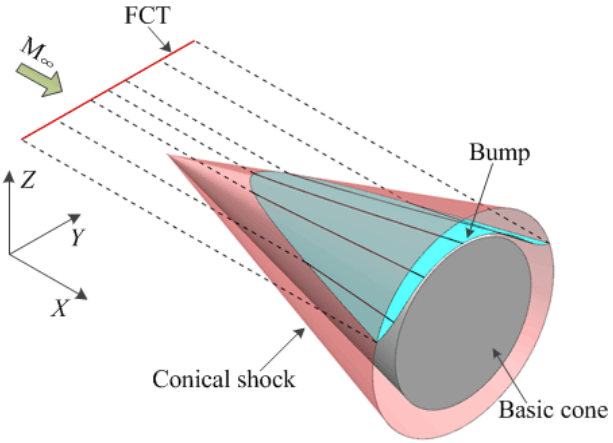


**Fig 1.** General sketch of a three-dimensional bump design

### 2.2. Numerical approach

The numerical simulation provided a highly effective tool for three-dimensional flow analysis. The present three-dimensional computational analysis of a hypersonic inlet flow including conical/normal shocks was carried out by using a numerical method that integrates the governing equations for structured grids with a second-order upwind method for the convection terms of the conservation equations. The flow was modelled with Reynolds-averaged Navier-Stokes equations for ideal gas, formulated as

$$\frac{\partial U}{\partial t} + \nabla \bullet F_t + \nabla \bullet F_V = Q \tag{1}$$

where $F_t$ and $F_v$ are the inviscid and viscous flux matrices respectively, and $Q$ represents the source vector.

In the present work, the shear stress transport (SST) turbulence model was selected to close Reynolds-averaged conservation equations because of its superior performance and stability as compared to other turbulence models for adverse pressure flows. And the compressible RANS system of equations was solved using the density based formulation with implicit algorithm of CFD code. To solve the governing equations, a point Gauss-Seidel scheme is used to perform time marching, and Roe's scheme in combination with the Monotone Upwind Scheme for Conservation Laws (MUSCL) interpolation method is adopted to obtain the inviscid fluxes at the control surfaces too.

### 2.3. Numerical approach verification

To verify the accuracy of the numerical approach mentioned above, the simulation of a swept compression ramp model [23] has been conducted in this chapter too. Similar to the bump model, the flow field around this model has obvious three-dimensional features. Thus, the reliability of the numerical approach used in this paper is approved by comparing the current simulation results and experiment data.

The schematic of swept compression ramp model is presented in Fig.2, where the swept angle $\lambda$ and streamwise compression angle $\alpha$ are $20^0$ and $16^0$ respectively. Fig.3 is the pressure ratio distribution along the wall at $Z$=69.9mm, $Z$=95.3mm and $Z$=120.7mm. In this graph, the coordinate origin indicates the leading edge point at each line. And meanwhile, the data at line $Z$=69.9mm and $Z$=120.7mm are moved forward and backward to 5mm respectively as shown in Fig.3. It can be found that the simulation results show a good agreement with the experiment data at each line. Therefore, the numerical approach used here is so precise that it is supposed to be adopted for following research.

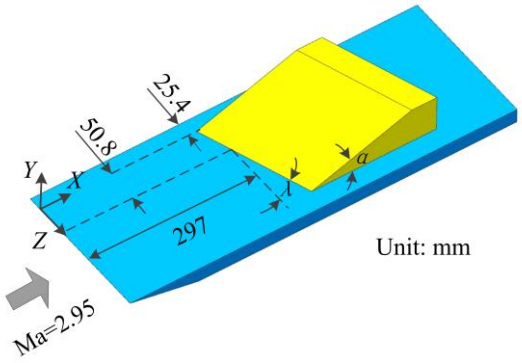


**Fig 2.** Schematic of swept compression ramp

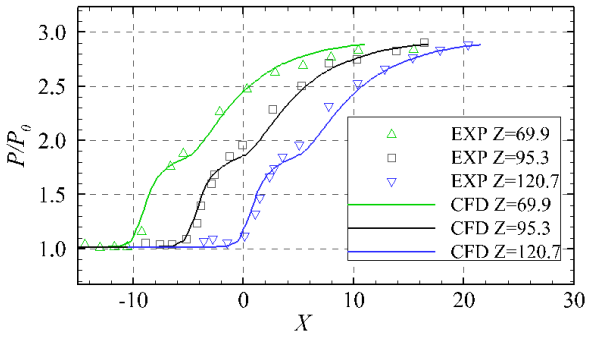


**Fig 3.** Surface pressure ratio distribution of swept compression ramp

## 3. Influence of 3D bump on the flow structure of hypersonic inlets

### 3.1. Hypersonic inlet models and grids

For the purpose of analysis, a typical hypersonic inlet was formed, termed "Type-1", with the design condition at Ma 6, angle-of-attack (AOA) $0^0$ and altitude 26 Km. Fig.4 presents the detailed parameters about it. Notably, the inlet is installed on the positive direction of Z axis for convenience as shown in Fig.4, while actually the hypersonic inlet is usually located under the high speed vehicles. So the negative direction of the Z axis is supposed to be the lift direction of the model in the subsequent simulations.

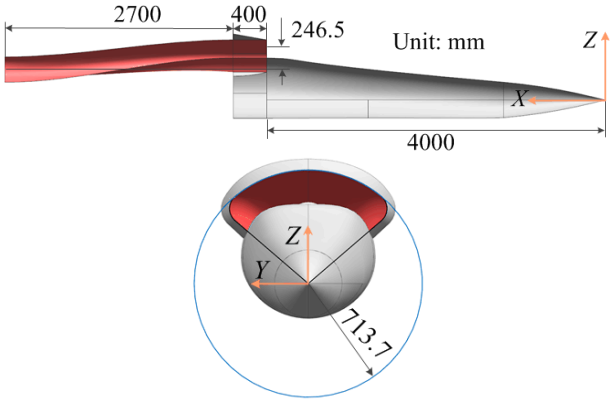


**Fig 4.** Schematic of Type-1

Correspondingly, streamlines tracing method mentioned above was utilised to produce a three-dimensional bump-compression surface as shown in Fig.5 (a), where $L$ = 1171.51 mm, $W$ = 974.92 mm and $H$ = 244.34 mm. Since the flow has been compressed by the front cone before, a non-uniform flow will exist upstream of the bump. In this case, the average Mach number after the front conical shock, equals to 5.3, was selected as the design Mach number and the shape of the conical shock generated by the bump was selected properly to ensure that the capture mass flow rate is basically the

same as Type-1. Then this slender bump has been integrated with Type-1 to create a new "Diverterless High-speed Inlet" as shown in Fig.5 (b). In order to assure the contrast effects, this paper just trims the bump and the forebody fuselage to ensure the shape of inlet internal surface hasn't been changed during the integration procedure. And as presented in Fig.5 (b), the blue part presents the original bump surface and the green part is the trimming surface. Throughout the whole paper, the term "Type-2" will refer to this novel hypersonic bump inlet.


(a) bump-compression surface (b) model of Type-2

**Fig 5.** Schematic of 3D bump surface and Type-2

In this study, only half geometry of Type-1 was used to generate the structured grid used for computations, since the flow field in it is assumed to be symmetric. The representative surface mesh for Type-1 is set out in Fig.6, where the orange part is the forebody fuselage, the green part represents the cowl, the red section indicates the inlet inner wall and the blue one is the symmetry plane. The grid system contains more than 3.1 million grid points and the viscous mesh employed a first-grid point placement from the wall at $y^+$ less than unity. Moreover, O-block was arranged throughout the whole inlet inner region and a stretching function was used to cluster grid points near the wall and shock locations to refine the grid system. The grid system of Type-2 is the same as Type-1.

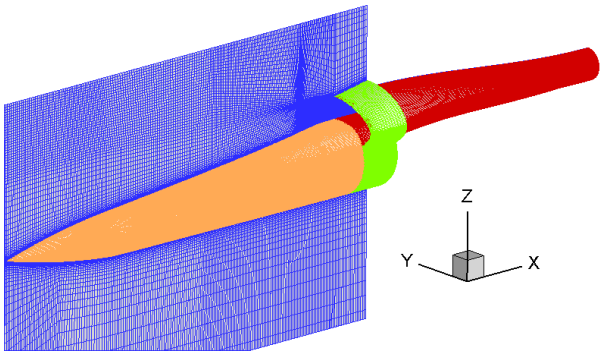


**Fig 6.** Surface mesh distribution on Type-1

For boundary conditions, no-slip velocity condition was enforced at the walls and pressure far field boundary condition was used at far field and the entrance section of the computational domain corresponding to the desired freestream Mach number and angle-of-attack. At the outflow boundary, where the airflow exits the computational, the back pressure was equal to the free stream pressure, which means the inlet works under the throughflow condition. Symmetry boundary condition was specified on the symmetry planes of the fuselages external domain and the intake internal domain (shown in Fig.6).

### 3.2. Flow characteristics analysis under design conditions (*Ma* = 6, *AOA* = $0^0$)

In this section, computations were carried out under design conditions to see the performance of two models. For the design conditions, the freestream Mach number is 6 and the cruising height is 26 Km with the angle-of-attack set to zero. At the height of 26 Km, the atmosphere parameters are used as the baseline values of the design, where $P_0$ = 2188.32 Pa, $T_0$ = 222.54 K and $\rho$ =0.034 kg/m$^3$.

Fig.7 presents the Mach number contour and streamlines distribution on the forebody fuselage for two models under design conditions. The most interesting aspect of this graph is that a majority of

streamlines within boundary layer are exhausted sideways to point B, outboard of inlet lip, upon Type-2 forebody fuselage, whereas the same thing doesn't take place on Type-1. In Fig.7 (b), it is apparent the bulk of streamlines are exiled out of the entrance, while a fraction of low-kinetic flow still gets into the inlet. This result, as shown in Fig.7, indicates that three-dimensional bump-compression is able to divert upstream boundary layer from inlet entrance efficiently, and reduce the quantity of low-kinetic flow inside correspondingly.

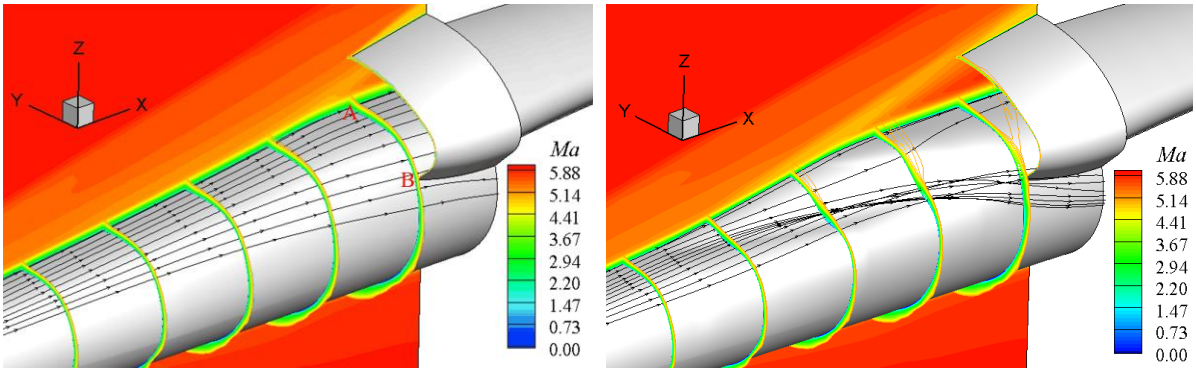


(a) Type-1 (b) Type-2

**Fig 7.** Mach contour and streamlines distribution on the forebody fuselage at design conditions

To have a better understanding of boundary layer circumstance, the boundary layer thickness was evaluated using a displacement thickness throughout the whole thesis. However, it is thought difficult to determine main flow behind the shock wave occurs from the bump edge. In this study, according to the literature [24], the boundary layer thickness is characterized using $\delta_{99\%}$ which is defined as the physical height of boundary layer at 99% of the freestream total pressure. And the free stream direction velocity and density at $\delta_{99\%}$ are defined as characteristic parameters. Hence the displacement thickness $\delta^*_{99\%}$ is calculated as

$$\delta^*_{99\%} = \int_0^h \left(1 - \frac{\rho u}{\rho_e u_e}\right) \mathrm{d}y \tag{2}$$

where $\rho$ and $u$ denote a distribution of density and freestream direction velocity in the boundary layer respectively, $\rho_e$ and $u_e$ are the characteristic parameters. Furthermore, $y$ represents the direction normal to the flat board, and the integral interval of $y$ direction is from a wall to $\delta_{99\%}$.

In view of that, Fig.8 shows the displacement thickness distribution at the inlet entrance section, where $Y/W$ = 0 is point A and $Y/W$ = -0.4 refers to point B in Fig.7 (a). As can be seen in this illustration, the displacement thickness of Type-2 is a bit higher than Type-1 at point B. A possible explanation for this might be that most of incoming boundary layer is blew sideways, and accumulates at point B. Around point A (-0.1< $Y/W$ <0), the height of boundary layer on Type-2 becomes thicker than Type-1 as well, because the surface here on Type-2 is the production of integration rather than the original bump-compression surface (see Fig.5 (2)). Hence, the incoming low-kinetic flow accumulates nearby too. In this work, the area, designated by displacement thickness curves and coordinate axes, is conducted to index upstream boundary layer intake. It is found that the dimensionless area value in Type-1 is approximately 0.00334, and Type-2 about 0.00303 by contrast. Therefore, the quantity of low-kinetic flow, ingested into Type-2 inlet, reduces by 9.3%. In other words, Type-2 has a better performance of redirecting boundary layer than Type-1 under design conditions.

Fig.9 compares the total pressure distribution throughout the inlet inner region of two models, where $\sigma$ means the total pressure recovery coefficient. From this graph, it can been seen that low-kinetic flow around point B ( $Y/W$ = -0.4~-0.2) gradually rotates to the symmetry plane at the first corner of the S-shape inlet thanks to the influence of the inlet profile. And then, this low-kinetic flow merges with the low-kinetic flow which comes from regions around point A ( $Y/W$ = -0.2~0) at cross-section 2 and hence an obvious separation bubble appears nearby. This separation bubble develops upward gradually along with the mainstream and its strength is gradually weakened. It is apparent that the separation

bubble inside the inlet of Type-2 is relatively smaller than Type-1 and its location is further forward as well. A probable explanation for this might be that the displacement thickness of the boundary layer for Type to is apparently smaller than Type-1 in the region around point B ( *Y/W* = -0.4~-0.2), as shown in Fig.8. This interesting finding indicates that the three-dimensional bump can diminish the separation to some extent by removing the incoming low-kinetic flow.

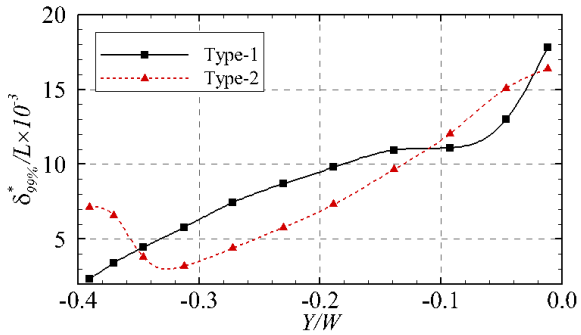


**Fig 8.** Boundary layer distribution at the inlet entrance section under design conditions

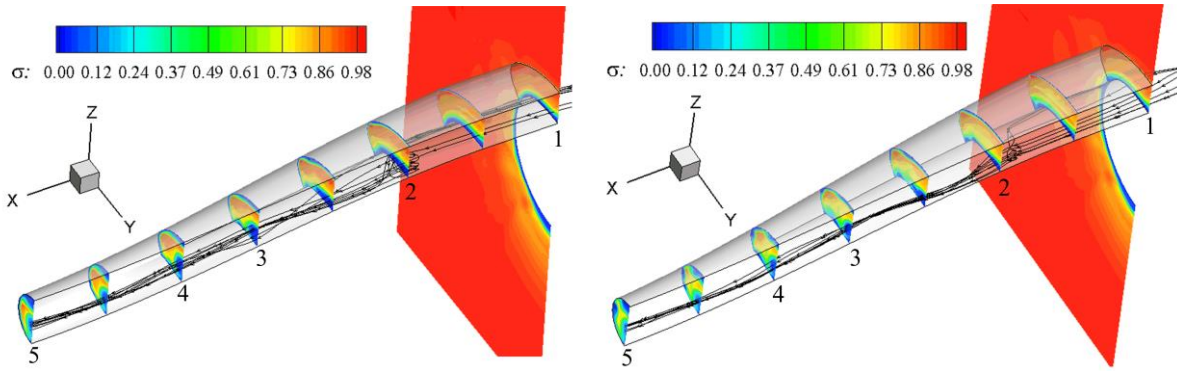


(a) Type-1 (b) Type-2

**Fig 9.** Contours of total pressure and streamlines inside the inlet at design conditions

Fig.10 further provides the Mach number distributions on the symmetry plane of two models under the design conditions, and the upper right plot is used to compare the size of the separation bubble. As can be seen in Fig.10, there is a significant difference between Type-1 and Type-2. The separation bubble of Type-1 ranges from 4.80 to 5.13 in the direction of *X/W* and the maximum value of *Z/W* is 0.53. As for Type-2, the separation region only ranges from 4.83 to 4.98 in the direction of *X/W* and the maximum value of *Z/W* is 0.51. As a consequence, it is obvious that the separation induced by the first cowl shock of Type-2 is smaller than that of Type-1 because of the influence of three-dimensional bump. And this finding is consistent with the previous analysis.

Meanwhile, it is interesting to note that there is an additional shock wave in front of the inlet entrance section in Type-2 (shock 2 in Fig.10 (b)). This shock wave is a conical shock generated by the bump-compression surface, and a Prandtl-Meyer expansion exist at the end of the bump because the shape of bump has been trimmed here. As a result, such a shock wave distribution in Type-2 might be the main reason for the decline of total pressure recovery coefficient.

The performance parameters of two models under the design conditions are summarized in Table 1. As can be seen from this table, two models have essentially the same capture mass flow rate with Type-2 only declined by 0.7%, which denotes that Type-2 meets the design requirement. Compared with Type-1, the overall compression ratio of Type-2 increases by 1.1%, the outlet Mach number decreases by 3.6% and the total pressure recovery coefficient decreases significantly, about 13%. The decline of total pressure recovery coefficient could be attributed to the additional conical shock wave mentioned above (as shown in Fig.10 (b)). In addition, the trimming process might also induce the loss of total pressure. And the current study found that the loss of total pressure predominantly takes place

in front of the inlet. In other words, the total pressure can be improved by optimizing the inlet inner surface which hasn't been changed in current work. And this is an important issue for future research.

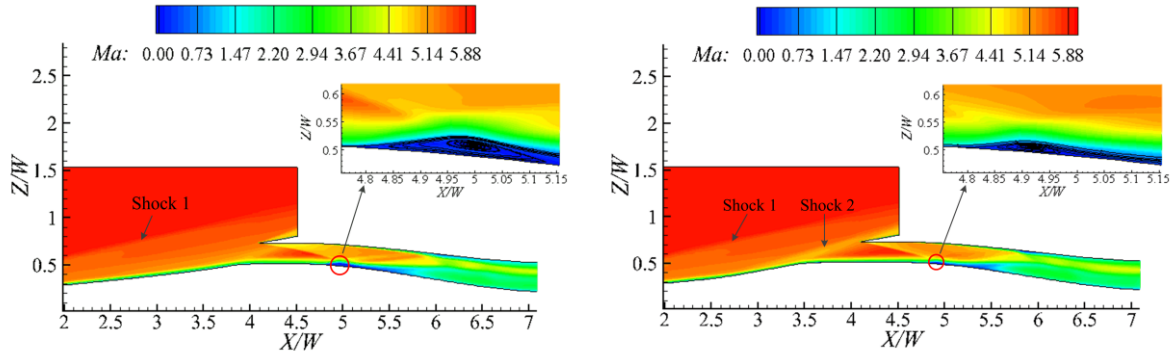


(a) Type-1 (b) Type-2

**Fig 10.** Contours of Mach number on the symmetry plane of two models at the design conditions

**Table 1.** Performance parameters comparison at the design conditions

| **Model** | $\dot{m}_{out}$ (kg/s) | $\sigma$ | $P_e$ / $P_0$ | $Ma_{out}$ |
|---|---|---|---|---|
| Type-1 | 8.15 | 0.46 | 14.45 | 3.03 |
| Type-2 | 8.10 | 0.40 | 14.61 | 2.92 |

### 3.3. Influence of 3D bump on the starting characteristic of hypersonic inlets

Then on the base of the previous analysis, this paper has compared the low-speed starting characteristics of two models under the design angle-of-attack (AOA = $0^0$) as well. Comprehensive numerical simulations at Ma = 3.5, AOA = $0^0$ have been performed to analyse the influence of a three-dimensional bump on the starting characteristics of hypersonic inlets. Fig.11 illustrates the Mach number contour and streamlines distribution on the forebody fuselage for two models at Mach 3.5. It is apparent that the shock has been pushed out of the inlet so that the whole inlet is choked and streamlines on the fuselage have to flow outside the cowl in Type-1 at Mach 3.5. By contrast, Type-2 can works successfully at Mach 3.5 and the bulk of boundary layer is displaced out of the cowl, which is the main reason why the inlet can start under this Mach number.

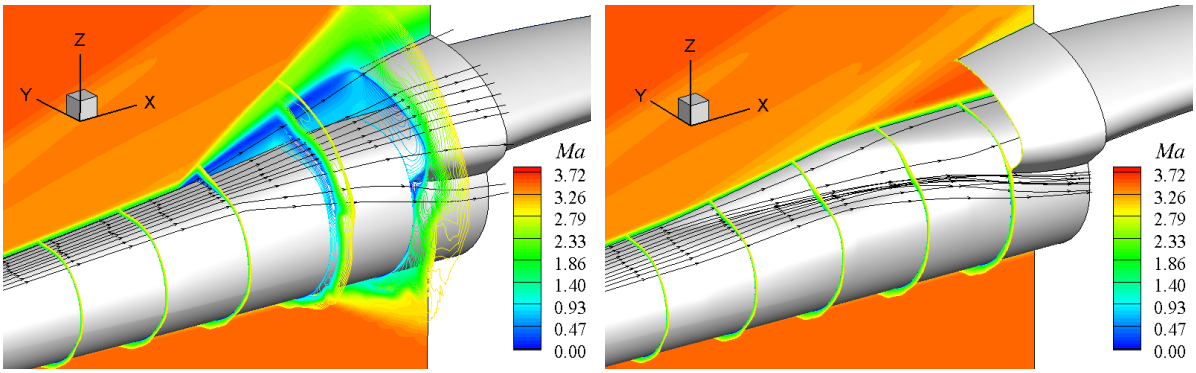


(a) Type-1 (b) Type-2

**Fig 11.** Mach contour and streamlines distribution on the inlet forebody at Ma = 3.5

And then Fig.12 further compares the Mach number distribution on the symmetry plane of two models at Ma = 3.5. As can be seen, the separation bubble of Type-1 has completely choked the inlet such that most of incoming flow can not get into the inlet. Hence, the unstarting characteristic is significant. As for Type-2, the bulk of incoming flow is able to flow freely throughout the inlet, and only a small separation bubbles appears at $X/W$ = 5.5.

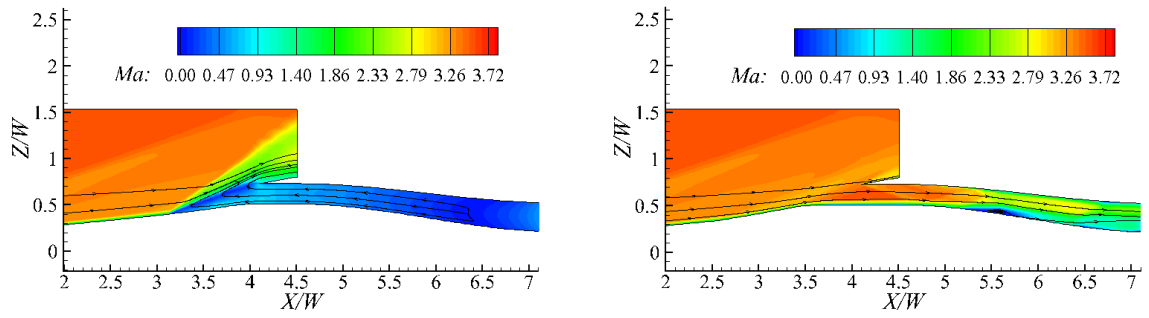


(a) Type-1 (b) Type-2

**Fig 12.** Contours of Mach number on the symmetry plane of two models at Ma = 3.5.

In general, these findings mentioned above indicates that a reasonable designed bump can suppress the separation significantly and provide a more homogeneous airflow inside the inlet under the condition that the capture mass flow rate is basically the same. On this basis, the low-speed starting characteristics of hypersonic inlets can be optimized obviously and the operating range of flight number can further be extended.

## 4. Influence of 3D bump on the aerodynamic performance of hypersonic inlets

In addition, the aerodynamic performances of two models were investigated, and then the influence of three-dimensional bump on the lift-drag characteristics of hypersonic inlets was analysed. The aerodynamic parameters considered in this study are the lift coefficient, drag coefficient and lift-to-drag ratio, and these two coefficients are normalized as follows:

$$C_L = \frac{L'}{q_\infty S_r} \tag{3}$$

$$C_D = \frac{D'}{q_\infty S_r} \tag{4}$$

Here, $L'$ and $D'$ are the lift and drag moment respectively, $S_r$ is the reference area and $q_\infty$ represents the freetream dynamic pressure.

The aerodynamic parameters of two models under the design conditions (Ma = 6, AOA = $0^0$) are presented in Table 2. It can be seen from the data in Table 2 that compared with the forebody of Type-1 (see Fig.6), both the lift coefficient and the drag coefficient of Type-2's forebody increase at the same time. However, the growth of the lift coefficient is less than the drag coefficient, resulting in the decrease of the lift-to-drag ratio by approximately 5.7%. As for the cowl part, the drag coefficients of two models are the same and the lift coefficient of Type-2 increases significantly. As a result, the lift-to-drag ratio of the cowl for Type-2 increases by about 6.5%. Then for the inlet section, both the lift coefficient and the drag coefficient of Type-2 grow simultaneously. The growth of the lift coefficient is obviously greater than the drag coefficient and consequently the lift-to-drag ratio increases by approximately 32.9%. In general, the overall lift-to-drag ratio of Type-2 is higher than Type-2 under the design conditions. The growth of the overall lift-to-drag ratio is about 16.7% and it is mainly related to the increase of the lift-to-drag ratio for the inlet section.

Fig.13 gives the lift coefficient characteristic curves of two models under the design Mach number 6, where curves in red represent Type-2 and the black curves indicate Type-1. Referring to Fig.13, the lift coefficient curves of two models coincide approximately at the cowl part. For the forebody section, the lift coefficient of Type-2 is slightly greater than that of Type-1 at various angles of attack. However for the lift coefficient of the inlet, the difference between two models varies a lot for different angles of attack. When the angle of attack is less than $4^0$, the lift coefficient of the inlet portion with Type-2 is greater than that of Type-1 and especially, the lift coefficient of the inlet portion with Type-2 is approximately 28.3% higher than Type-1. Subsequently, when the angle of attack is greater than $4^0$, the lift coefficient of the inlet portion with Type-2 is less than that of Type-1.

Based on the previous analysis, the difference between the lift coefficients of the inlet portions with two models might be the main factor causing the difference of the overall lift coefficients. Taken together, when the angle of attack is less than $4^0$, the overall lift coefficient of Type-2 is greater than that of Type-1. Especially, compared with Type-1, the overall lift coefficient of Type-2 increases by about 25.8%. On the other hand, the overall lift coefficient of Type-2 is less than that of Type-1 under the condition that the angle of attack is greater than $4^0$.

**Table 2.** Aerodynamic parameters of two models at the design conditions

| | | $C_L$ | $C_D$ | $L/D$ |
|---|---|---|---|---|
| Type-1 | Forebody | 0.068 | 0.035 | 1.94 |
| | Cowl | 0.044 | 0.016 | 2.77 |
| | Inlet | -0.046 | 0.049 | -0.94 |
| | Total | 0.066 | 0.100 | 0.66 |
| Type-2 | Forebody | 0.070 | 0.038 | 1.83 |
| | Cowl | 0.046 | 0.016 | 2.95 |
| | Inlet | -0.033 | 0.054 | -0.63 |
| | Total | 0.083 | 0.108 | 0.77 |

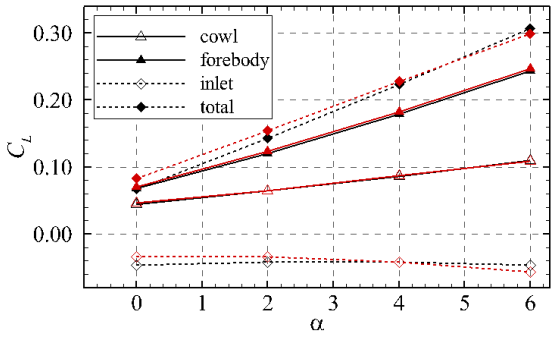


**Fig 13.** Characteristic curves of the lift coefficient at Ma = 6.

The drag coefficient characteristic curves of two models are presented in Fig.14, and curves in red represent Type-2 while the black curves are Type-1. As can be seen in this graph, the drag coefficient of the cowl with Type-2 is slightly greater than that of Type-1 at various angles of attack. As for the other two parts (the forebody and the inlet), the drag coefficient of Type-2 is obviously higher than that of Type-1 at each angle of attack. As a consequence, the total drag coefficient of Type-2 is greater than that of Type-1 at each angle of attack. And, compared with Type-1, the overall drag coefficient of Type-2 increases by approximately 8%.

Fig.15 further compares the lift-to-drag ratio characteristics of two models at Ma = 6, where the red curves indicate Type-2 and the black curves represent Type-1. From this graph, we can see that the lift-to-drag ratio of the cowl section with Type-2 is larger than that of Type-1 at all angles of attack, and the difference between two models declines with the growth of the angle of attack. For the forebody portion, the lift-to-drag ratio of Type-2 is less than that of Type-1 at each angle of attack, and the difference between them are almost the same at all angles of attack. Then as for the inlet portion, the lift-to-drag ratio of Type-2 is greater than that of Type-1 when the angle of attack is less than $4^0$. Especially, the lift-to-drag ratio of the inlet portion with Type-2 increases by approximately 32.9% compare with Type-1 at the design conditions. And when the angle of attack is greater than $4^0$, the lift-to-drag ratio of the inlet portion with Type-2 becomes less than that of Type-1.

Hence in the aspect of the overall lift-to-drag ratio of two models, it can be found that the overall lift-to-drag ratio of two models coincides closely in the range of $2^0$ angle of attack to $4^0$ angle of attack. When the angle of attack is less than $2^0$, the total lift-to-drag ratio of Type-2 is greater than that of

Type-1 and the value of Type-2 increases by about 16.7% compared with that of Type-1 at the design angle of attack. Then if the angle of attack is greater than $4^0$, the total lift-to-drag ratio of Type-2 turns out to be less than that of Type-1.

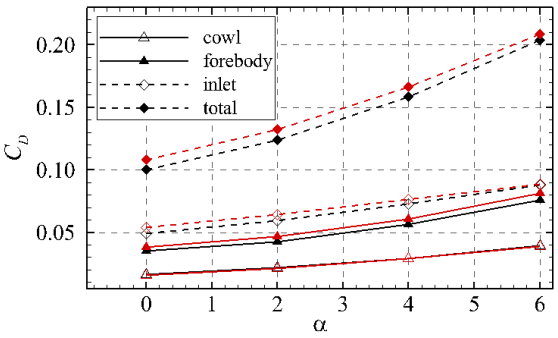


**Fig 14.** Characteristic curves of the drag coefficient at Ma = 6.

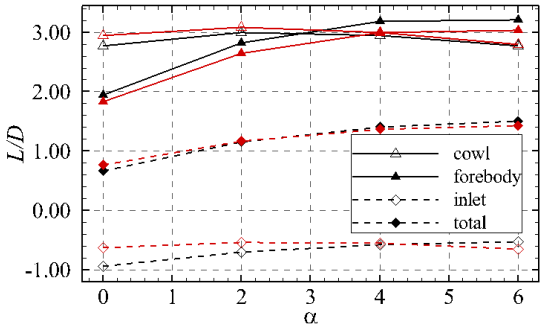


**Fig 15.** Characteristic curves of the lift-to-drag ratio at Ma = 6.

Together these results provide important insights into the influence of the three-dimensional bump on the aerodynamic performance of the hypersonic inlet. Under the design conditions, the overall lift-to-drag ratio of Type-2 increases significantly by about 16.7% compared with the overall lift-to-drag ratio of Type-1. The presence of the three-dimensional bump does have a negative effect on the lift-to-drag ratio of the forebody portion. However, the lift-to-drag ratio of the inlet portion and the cowl portion increases significantly with the existence of the bump so that the overall lift-to-drag ratio of Type-2 is greater than that of Type-1.

## 5. Conclusion

In the present work, a cone-derived bump-compression surface was installed on the forebody fuselage of a typical hypersonic inlet under the design conditions with Ma = 6 and AOA = $0^0$. Comprehensive numerical simulations have been carried out to study the influence of the three-dimensional bump on the flow structure and the low-speed starting characteristics of the hypersonic inlet. At the same time, the influence of the bump on the aerodynamic performance of the hypersonic inlet is discussed detailedly as well. The results are as follows:

(1) Under the design conditions, the boundary layer is displaced significantly by the bump and the quantity of low-kinetic flow ingested into the inlet with Type-2 is reduced by approximately 9.3% compared with Type-1. As a consequence, the separation inside the inlet can be suppressed effectively.

(2) At the design angle of attack, Type-2 is able to work successfully while the inlet of Type-1 is completely choked by the large separation bubble. Hence, it can be concluded that a reasonable designed bump is able to optimize the low-speed starting performance of the hypersonic inlet significantly and reduce the starting Mach number as well.

(3) Under the design conditions, the overall lift-to-drag ratio of Type-2 increases by about 16.7% compared that of Type-1. Although the presence of the bump has a negative influence on the lift-

to-drag ratio of the forebody portion, the bump can heighten the lift-to-drag ratio of the cowl portion and the inlet portion obviously. Therefore, the overall lift-to-drag ratio of the hypersonic inlet can be improved with the existence of the three-dimensional bump under the design conditions.

## References


1. Mayer D W, Paynter G C.: Prediction of supersonic inlet unstart caused by freestream disturbances[J]. Aiaa Journal, 2012, 33(2):266-275.
2. Hawkins W, Marquart E.: Two-dimensional generic inlet unstart detection at Mach 2.5-5.0[C]// International Aerospace Planes and Hypersonics Technologies. 2013.
3. Rodi P E, Emami S, Trexler C A.: Unsteady pressure behavior in a ramjet/scramjet inlet[J]. Journal of Propulsion & Power, 2012, 12(3):486-493.
4. Shimura T, Mitani T, Sakuranaka N, et al.: Load Oscillations Caused by Unstart of Hypersonic Wind Tunnels and Engines[J]. Journal of Propulsion & Power, 2012, 14(3):348-353.
5. S. O, Byrne, Doolan M, et al. Analysis of Transient Thermal Choking Processes in a Model Scramjet Engine[J]. Journal of Propulsion & Power, 2000, 16(5):808-814.
6. Wagner J, Yuceil K, Valdivia A, et al.: PIV Measurements of the Unstart Process in a Supersonic Inlet/Isolator[C]// Fluid Dynamics Conference and Exhibit. 2008:1002-1003.
7. Do H, Im S K, Mungal M G, et al.: The influence of boundary layers on supersonic inlet flow unstart induced by mass injection[J]. Experiments in Fluids, 2011, 51(3):679-691.
8. E T Curran, W H Heiser, and, D T Pratt.: Fluid Phenomena in Scramjet Combustion Systems[J]. Annual Review of Fluid Mechanics, 2003, 28(1):323-360.
9. Sato S, Izumikawa M, Tomioka S, et al.: Scramjet engine test at the Mach 6 flight condition[C]// Joint Propulsion Conference and Exhibit. 2013.
10. Wang X, Le J.: Computations of inlet/isolator for SCRAMjet engine[J]. Journal of Thermal Science, 2000, 9(4):334-338.
11. Tam C J, Eklund D, Behdadnia R.: Influence of Downstream Boundary Conditions on Scramjet-Isolator Simulations[C]// Aiaa Applied Aerodynamics Conference. 2006.
12. Kodera H, Tomioka S, Kanda T, et al.: Mach 6 Test of a Scramjet Engine with Boundary-Layer Bleeding[J].
13. Yuceil K, Valdivia A, Wagner J, et al.: Active Control of Supersonic Inlet Unstart Using Vortex Generator Jets[C]// Aiaa Fluid Dynamics Conference. 2009.
14. Simon P C, Brown D W, Huff R G.: Performance of external-compression bump inlet at Mach numbers of 1.5 and 2.0[J]. Technical Report Archive & Image Library, 1957.
15. Goldsmith, E. L.: Intake aerodynamics[M]. American Institute of Aeronautics and Astronautics, 1985.
16. Ferri A.: Supersonic flow around circular cones at angles of attack[J]. Technical Report Archive & Image Library, 1951, 79(5):P5–P5.
17. Gridley, M. C., and Cahill, M.J.: ACIS air induction system trade study[J]. AIAA Journal, 1996.
18. Sang D K, Dong J S.: Numerical study on performance of supersonic inlets with various three-dimensional bumps[J]. Journal of Mechanical Science & Technology, 2008, 22(8):1640-1647.
19. Saheby E B, Huang G, Qiao W, et al.: A novel aerodynamic surface for redirecting the boundary layer[C]// Aiaa Applied Aerodynamics Conference. 2013.
20. Hamstra, J. W., McCallum, B. N., McFarlan, J. D., and Moorehouse, J.A.: Development, Verification, and Transition of an Advanced Engine Inlet Concept for Combat Aircraft Application, Lockheed Martin Aerospace Corp. Paper MP-121-P-43, 2003

21. K. G. Bowcutt.: Optimization of Hypersonic Waveriders Derived from Cone Flows including Viscous Effects (Ph.D), University of Maryland, College Park, 1986.
22. Taylor G I, Maccoll J W. The Air Pressure on a Cone Moving at High Speeds. II[J]. Proceedings of the Royal Society A Mathematical Physical & Engineering Sciences, 1933, 139(139):298-311.
23. Settles G S， Teng H Y. Cylindrical and conical flow re-gimes of three-dimensional shock/boundary layer in-teractions[J]. AIAA Journal, 2012, 22(2):194-200.
24. Miki H, Watanabe Y, Kameda M. Performance evalua-tion of a boundary layer diverter for supersonic propul-sion system[R]. 28TH Inter-national Congress of the Aer-onautical Sciences, 2012.